

Supplement of

Iron from coal combustion particles dissolves much faster than mineral dust under simulated atmospheric acid conditions

Clarissa Baldo et al.

5 *Correspondence to:* Zongbo Shi (z.shi@bham.ac.uk); Akinori Ito (akinori@jamstec.go.jp)

Table S1: Summary of the Fe dissolution experiments conducted in this study. A dust/liquid ratio of 1 g L⁻¹ was used at different experimental conditions. The molar concentrations of H₂SO₄, H₂C₂O₄ and (NH₄)₂SO₄ in the experiment solutions are reported (mol L⁻¹). The molar concentration and activity (a) of H⁺ and the solution pH before adding the samples (i) and at the end of the experiments (f) were calculated using the E-AIM model III for aqueous solution (Wexler and Clegg, 2002). The estimated buffered H⁺ is ~0.008 M for Krakow ash, ~0.0007 M for Aberthaw/Shandong ash, ~0.004 M for Libya dust (the procedure used to calculate the sample buffer capacity is reported in section 2.2). The final pH (pH_f) accounts for the buffer capacity of the CFA samples. For the experiment solutions with no (NH₄)₂SO₄, the initial pH (pH_i) and pH_f were also measured

	Exp.	[H ₂ SO ₄]	[(NH ₄) ₂ SO ₄]	[H ₂ C ₂ O ₄]	Model estimates						Measured pH	
					[H ⁺] _i	[H ⁺] _f	a(H ⁺) _i	a(H ⁺) _f	pH _i	pH _f	pH _i	pH _f
Krakow ash	Exp 1	0.01	-	-	0.016	0.009	0.86	0.86	1.9	2.1	1.9	2.1
	Exp 2	0.05	1	-	0.031	0.029	0.29	0.29	2.0	2.1	0.0	-
	Exp 3	0.05	1	0.01	0.035	0.032	0.29	0.29	2.0	2.0	0.0	-
	Exp 4	0.01	-	0.01	0.023	0.016	0.86	0.85	1.7	1.9	1.7	1.9
	Exp 1	0.005	-	-	0.008	0.002	0.89	0.88	2.1	2.7	2.2	2.6
	Exp 2	0.01	1	-	0.006	0.004	0.28	0.28	2.8	3.0	0.0	-
	Exp 3	0.005	1	0.01	0.007	0.005	0.28	0.28	2.7	2.9	0.0	-
	Exp 5	0.1	-	0.03	0.138	0.131	0.76	0.76	1.0	1.0	1.1	1.1
	Exp 6	0.25	0.5	0.03	0.189	0.186	0.49	0.49	1.0	1.0	0.0	-
	Exp 7	0.35	1	0.03	0.252	0.249	0.39	0.39	1.0	1.0	0.0	-
Exp 8	0.4	1.5	0.03	0.285	0.282	0.33	0.33	1.0	1.0	0.0	-	
Aberthaw ash	Exp 1	0.005	-	-	0.008	0.008	0.89	0.89	2.1	2.2	2.1	2.3
	Exp 2	0.05	1	-	0.031	0.031	0.29	0.29	2.0	2.0	0.0	-
	Exp 3	0.05	1	0.01	0.035	0.034	0.29	0.29	2.0	2.0	0.0	-
	Exp 4	0.002	-	0.01	0.012	0.011	0.90	0.90	2.0	2.0	2.0	2.1
	Exp 1	0.001	-	-	0.002	0.001	0.94	0.94	2.8	2.9	2.8	3.1
	Exp 2	0.005	1	-	0.003	0.003	0.28	0.28	3.1	3.1	0.0	-
Shandong ash	Exp 1	0.005	-	-	0.008	0.008	0.89	0.89	2.1	2.2	2.1	2.2
	Exp 2	0.05	1	-	0.031	0.031	0.29	0.29	2.0	2.0	0.0	-
	Exp 3	0.05	1	0.01	0.035	0.034	0.29	0.29	2.0	2.0	0.0	-
	Exp 4	0.002	-	0.01	0.012	0.011	0.90	0.90	2.0	2.0	2.0	2.0
	Exp 1	0.001	-	-	0.002	0.001	0.94	0.94	2.8	2.9	2.8	3.1
	Exp 2	0.005	1	-	0.003	0.003	0.28	0.28	3.1	3.1	0.0	-

Libya dust	Exp 1	0.01	-	-	0.016	0.012	0.86	0.86	1.9	2.0	1.9	2.0
	Exp 2	0.05	1	-	0.031	0.030	0.29	0.29	2.0	2.1	0.0	-
	Exp 3	0.05	1	0.01	0.035	0.033	0.29	0.29	2.0	2.0	0.0	-
	Exp 4	0.005	-	0.01	0.016	0.012	0.88	0.87	1.9	2.0	1.9	2.0

Table S2: Summary of the molar concentration in mol L⁻¹ and activity (a) of total oxalate ions, C₂O₄²⁻, and HC₂O₄⁻ in the experiment solutions calculated using the E-AIM model III for aqueous solution (Wexler and Clegg, 2002). A comprehensive description of the experimental conditions is provided in Table S1. pH_f is the calculated final pH in the experiment solutions.

Sample	Exp.	pH _f	[oxalate] _{total}	[C ₂ O ₄ ²⁻]	a(C ₂ O ₄ ²⁻)	[HC ₂ O ₄ ⁻]	a(HC ₂ O ₄ ⁻)
Krakow ash	Exp 3	2.0	0.009	0.00071	0.04	0.009	0.55
Krakow ash	Exp 4	1.9	0.008	0.00006	0.49	0.008	0.86
Krakow ash	Exp 3	2.9	0.010	0.00343	0.04	0.006	0.54
Krakow ash	Exp 5	1.0	0.012	0.00002	0.22	0.012	0.79
Krakow ash	Exp 6	1.0	0.015	0.00010	0.06	0.015	0.64
Krakow ash	Exp 7	1.0	0.015	0.00015	0.04	0.015	0.65
Krakow ash	Exp 8	1.0	0.015	0.00022	0.03	0.015	0.68
Aberthaw ash	Exp 3	2.0	0.009	0.00066	0.04	0.009	0.56
Aberthaw ash	Exp 4	2.0	0.009	0.00007	0.60	0.009	0.90
Shandong ash	Exp 3	2.0	0.009	0.00066	0.04	0.009	0.56
Shandong ash	Exp 4	2.0	0.009	0.00007	0.60	0.009	0.90
Libya dust	Exp 3	2.0	0.009	0.00068	0.04	0.009	0.56
Libya dust	Exp 4	2.0	0.008	0.00006	0.55	0.008	0.88

25 **Table S3: Constants used to calculate the Fe dissolution rates for fossil fuel combustion aerosols in Ito (2015), and the new dissolution scheme implemented in this study. Note that the dissolution scheme in Ito (2015) was based on laboratory measurements conducted at low ionic strength.**

Scheme	Reference	Rate constant - $k(\text{pH}, T)^a$		m^c
Proton	Ito (2015)	$5.24 \times 10^{-8} \exp[E(\text{pH})^b \times (1/298 - 1/T)]$		0.36
Oxalate	Ito (2015)	$3.85 \times 10^{-6} \exp[E(\text{pH})^b \times (1/298 - 1/T)]$		1
Photoinduced	Ito (2015)	$4.10 \times 10^{-6} \exp[E(\text{pH})^b \times (1/298 - 1/T)]$		1
Proton	This study	$7.61 \times 10^{-6} \exp[E(\text{pH})^b \times (1/298 - 1/T)]$	Stage I - Kinetic fast	0.241
		$1.91 \times 10^{-7} \exp[E(\text{pH})^b \times (1/298 - 1/T)]$	Stage II - Kinetic intermediate	0.195
		$2.48 \times 10^{-7} \exp[E(\text{pH})^b \times (1/298 - 1/T)]$	Stage III - Kinetic slow	0.843
Proton + Oxalate	This study	$5.54 \times 10^{-6} \exp[E(\text{pH})^b \times (1/298 - 1/T)]$	Stage I - Kinetic fast	0.209
		$1.50 \times 10^{-7} \exp[E(\text{pH})^b \times (1/298 - 1/T)]$	Stage II - Kinetic intermediate	0.091
		$1.77 \times 10^{-8} \exp[E(\text{pH})^b \times (1/298 - 1/T)]$	Stage III - Kinetic slow	0.204

^a $K(\text{pH}, T)$ is the rate constant (moles Fe $\text{g}^{-1} \text{s}^{-1}$) for each dissolution scheme.

^b $E(\text{pH}) = -1.56 \times 10^3 \times \text{pH} + 1.08 \times 10^4$.

^c m_i is the reaction order with respect to aqueous phase protons.

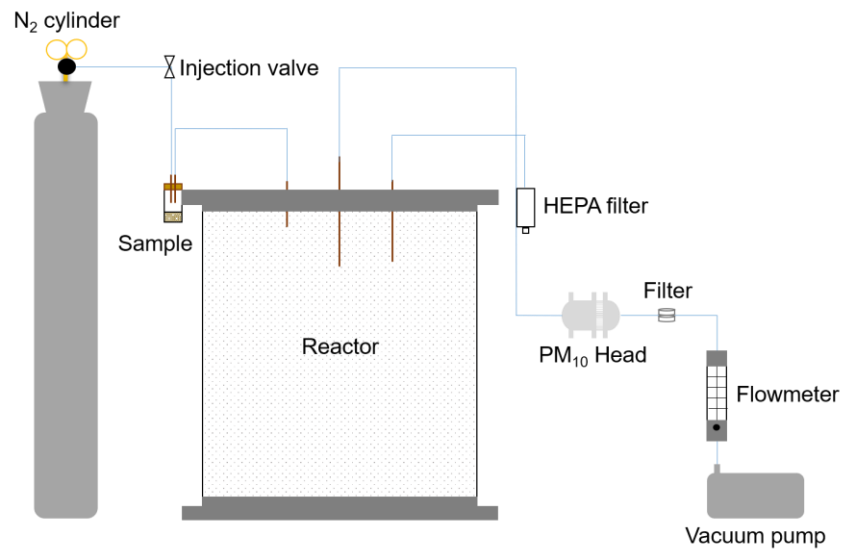
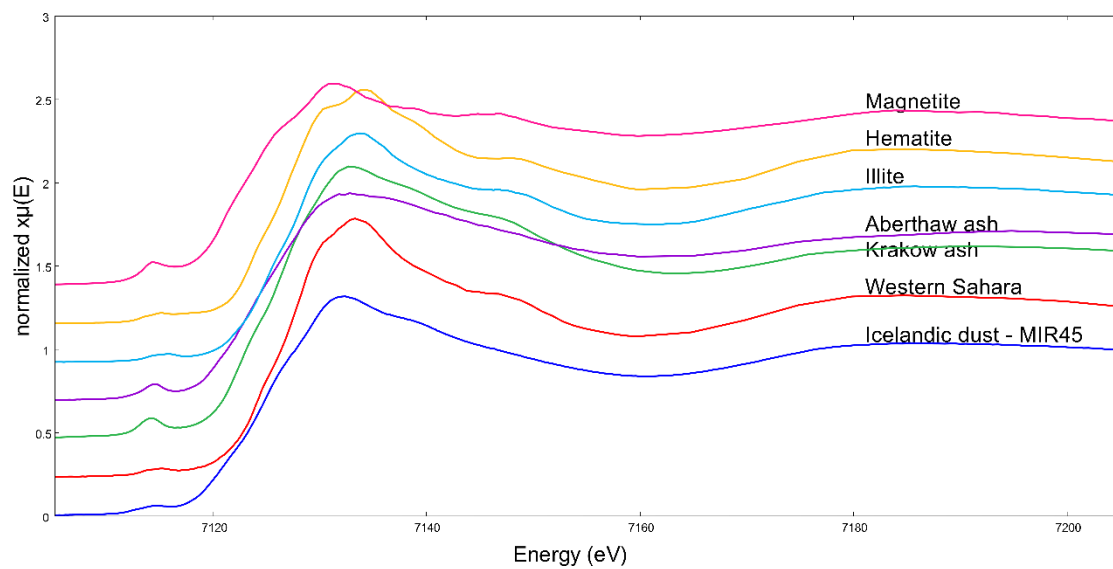
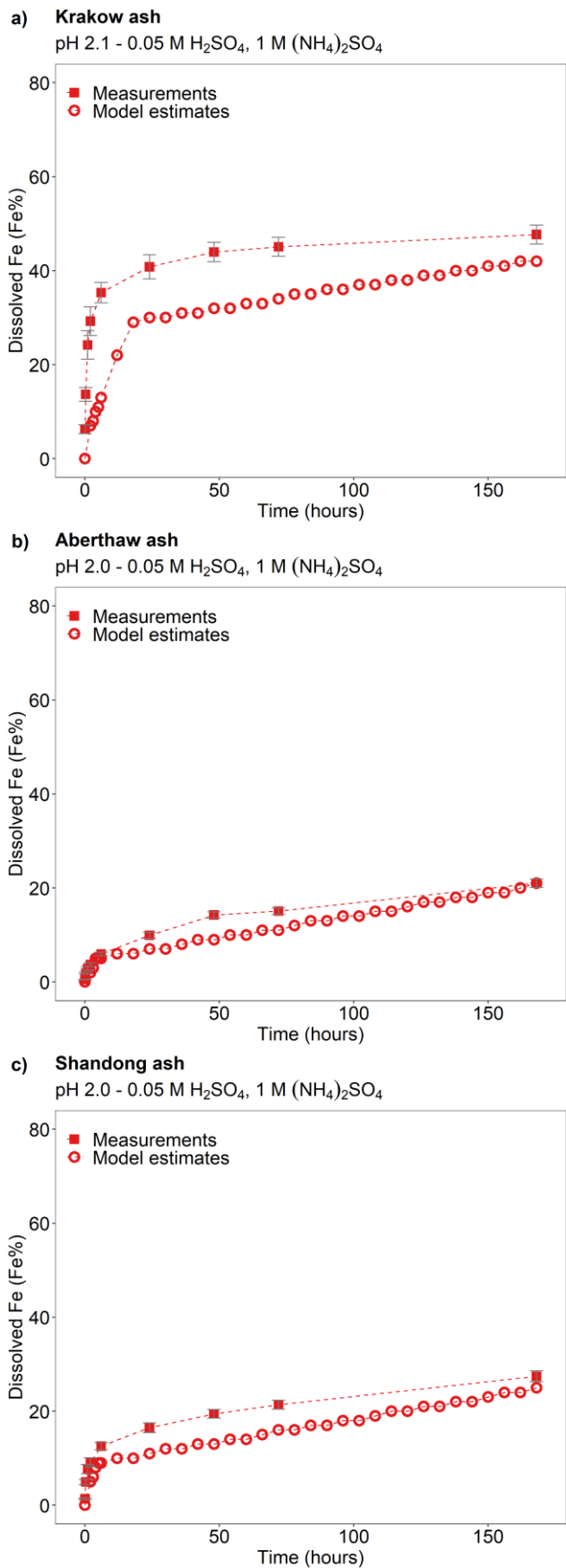


Figure S1: PM₁₀ collection system.



35 **Figure S2: Fe K-edge XANES spectra of Krakow ash, Aberthaw ash, magnetite, hematite, and illite standards, Icelandic dust (sample MIR 45) and northern African dust (western Sahara).**



40 Figure S3: Comparison between the Fe dissolution kinetics of a) Krakow ash, b) Aberthaw ash and c) Shandong ash predicted using Eq. (1) and measured in H₂SO₄ solutions at around pH 2 with 1 M (NH₄)₂SO₄ in the experiment solutions are shown. The molar concentrations of H₂SO₄ and (NH₄)₂SO₄ in the experiment solutions are shown. The final pH of the experiment solutions is also reported, which was calculated using the E-AIM model III for aqueous solution (Wexler and Clegg, 2002) accounting for the buffer capacity of the CFA samples (Experiments 2 at around pH 2 in Table S1).

45

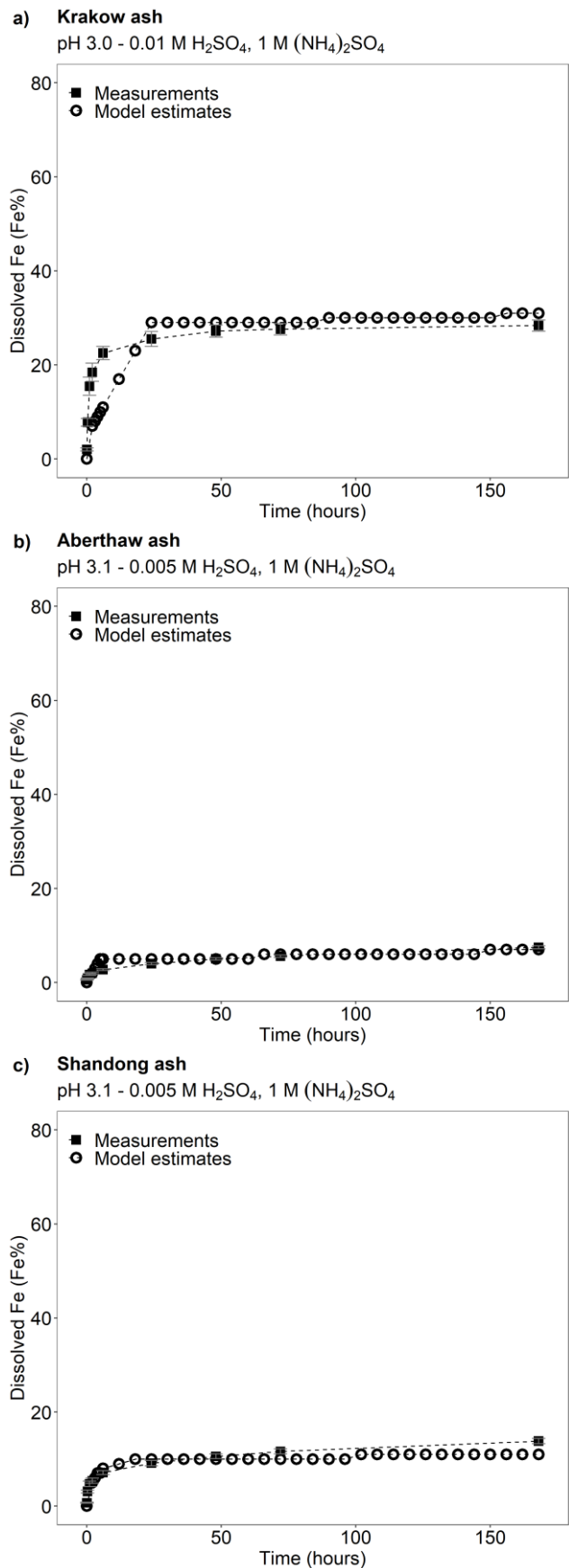
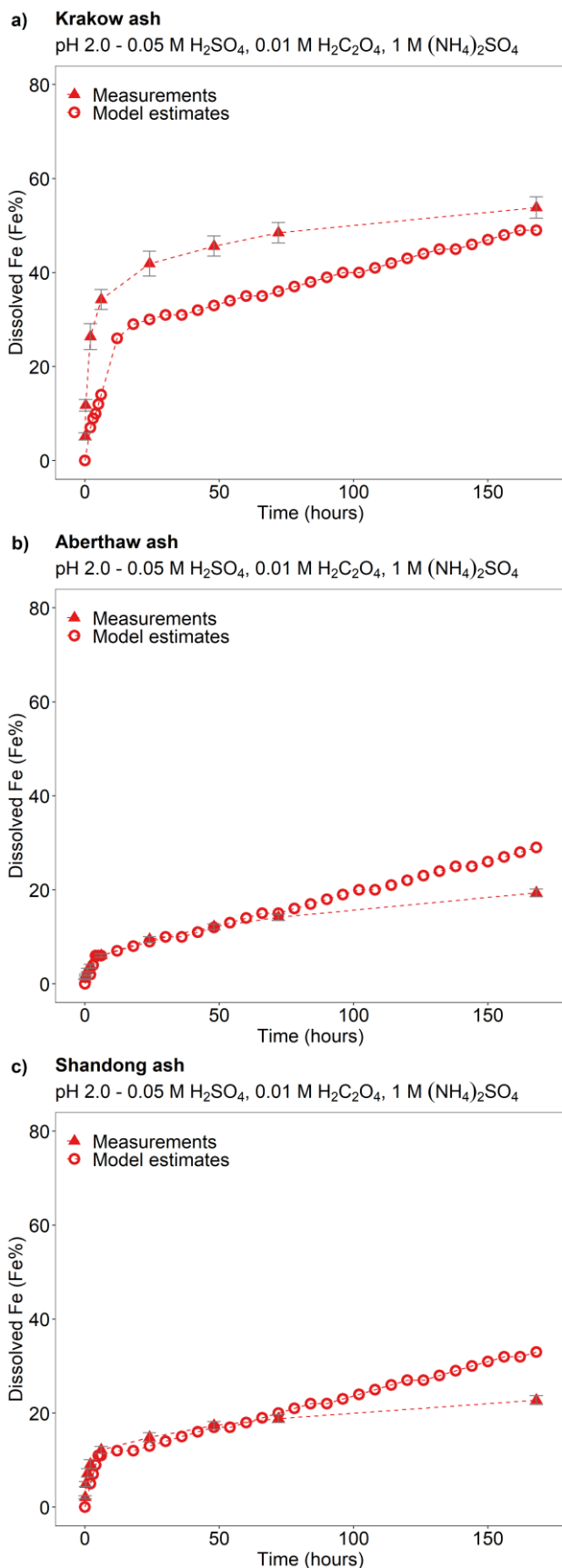
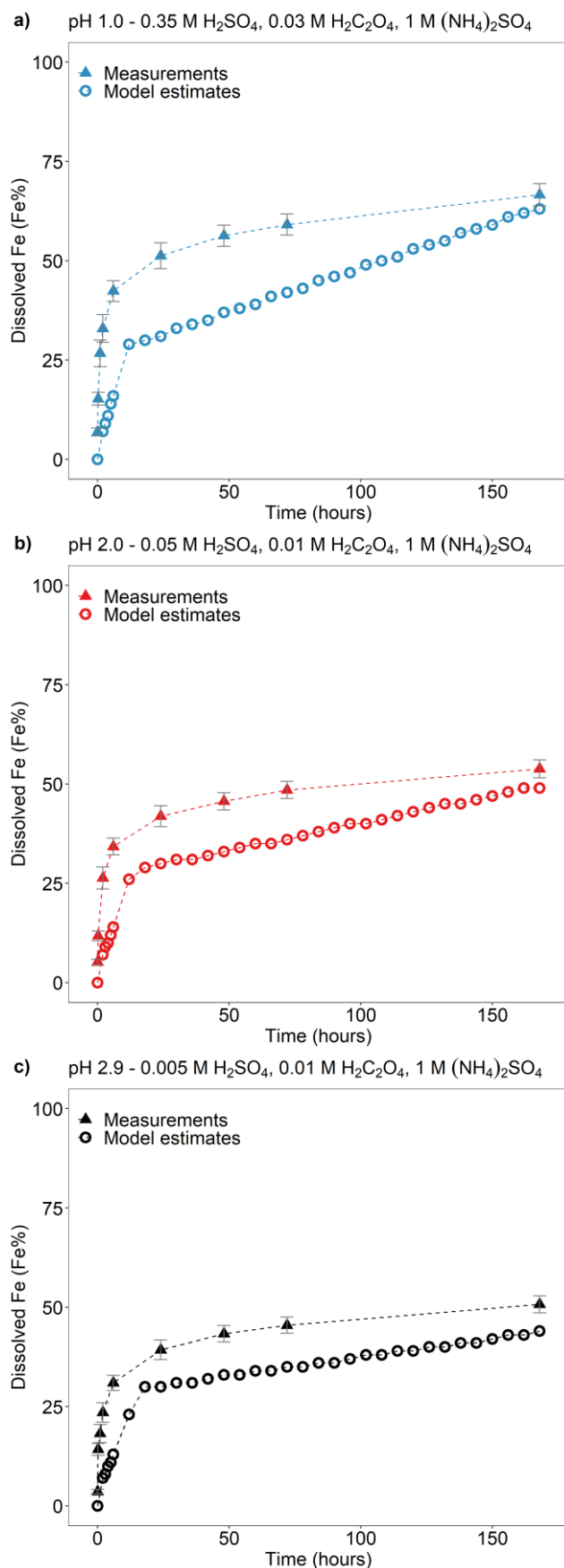


Figure S4: Comparison between the Fe dissolution kinetics of a) Krakow ash, b) Aberthaw ash and c) Shandong ash predicted using Eq. (1) and measured in H₂SO₄ solutions at around pH 3 with 1 M (NH₄)₂SO₄ in the experiment solutions are shown. The molar concentrations of H₂SO₄ and (NH₄)₂SO₄ in the experiment solutions are shown. The final pH of the experiment solutions is also reported, which was calculated using the E-AIM model III for aqueous solution (Wexler and Clegg, 2002) accounting for the buffer capacity of the CFA samples (Experiments 2 at around pH 3 in Table S1).

50



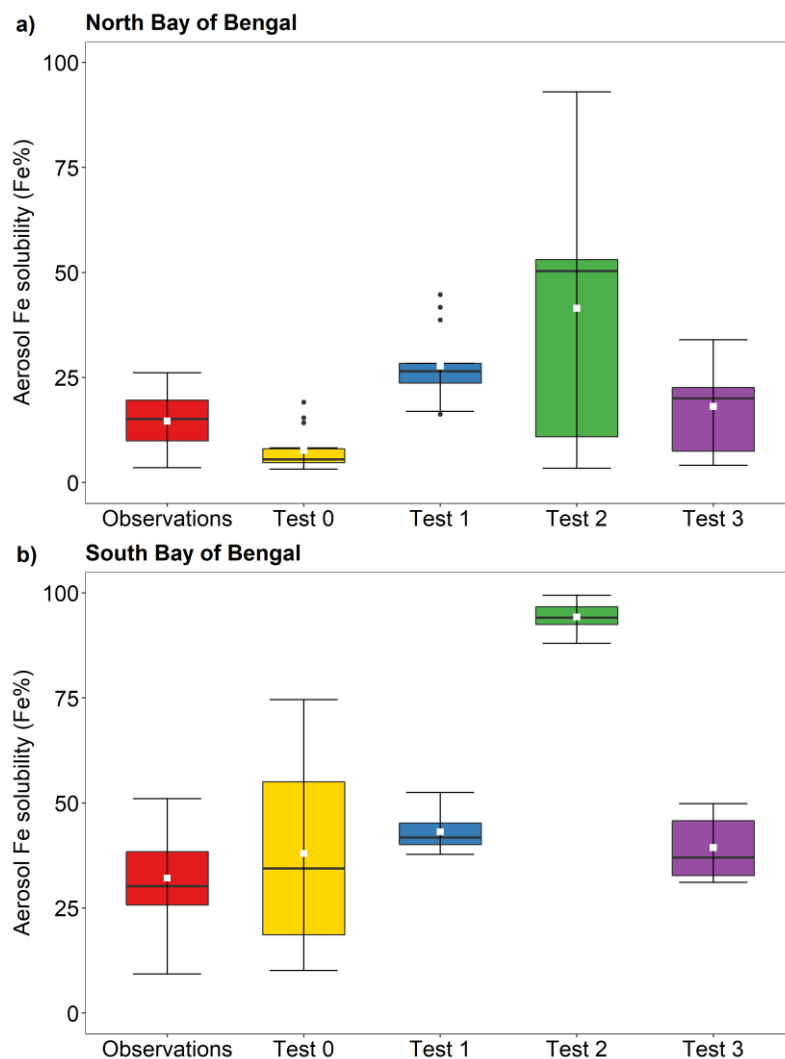
55 **Figure S5: Comparison between the Fe dissolution kinetics of a) Krakow ash, b) Aberthaw ash and c) Shandong ash predicted using Eq. (1) and measured in H₂SO₄ solutions at pH 2.0 with 0.01 M H₂C₂O₄ and 1 M (NH₄)₂SO₄. The molar concentrations of H₂SO₄, H₂C₂O₄ and (NH₄)₂SO₄ in the experiment solutions are shown. The final pH of the experiment solutions is also reported, which was calculated using the E-AIM model III for aqueous solution (Wexler and Clegg, 2002) accounting for the buffer capacity of the CFA samples (Experiments 3 at pH 2.0 in Table S1).**



60

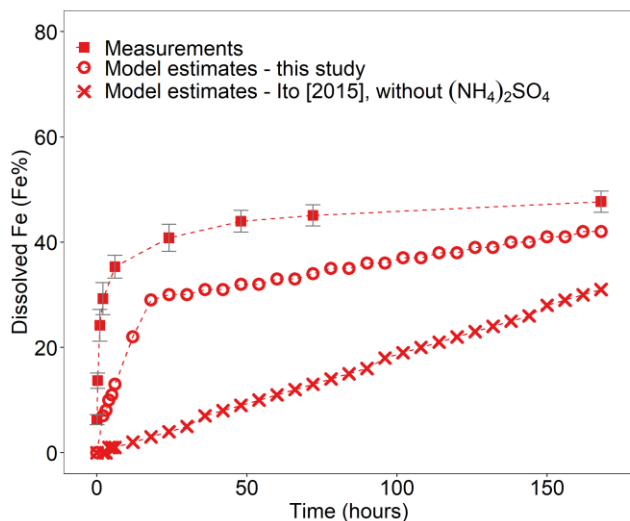
Figure S6: Comparison between the Fe dissolution kinetics of Krakow ash predicted using Eq. (1) and measured in H₂SO₄ solutions a) at pH 1.0 with 0.03 M H₂C₂O₄ and 1 M (NH₄)₂SO₄, b) at pH 2.0 with 0.01 M H₂C₂O₄ and 1 M (NH₄)₂SO₄, c) at pH 2.9 with 0.01 M H₂C₂O₄ and 1 M (NH₄)₂SO₄. The molar concentrations of H₂SO₄, H₂C₂O₄ and (NH₄)₂SO₄ in the experiment solutions are shown. The final pH of the experiment solutions is also reported, which was calculated using the E-AIM model III for aqueous solution (Wexler and Clegg, 2002) accounting for the buffer capacity of the CFA samples (Experiment 7 at pH 1.0, Experiment 3 at pH 2.0, and Experiment 3 at pH 2.9 in Table S1).

65

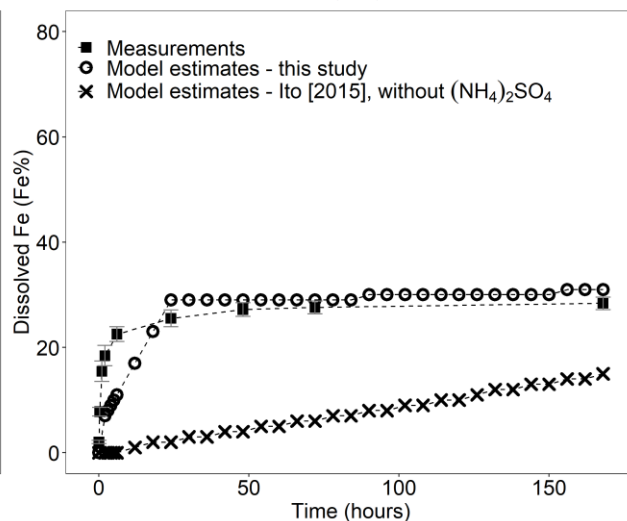


70 **Figure S7: Average Fe solubility in PM_{2.5} aerosol particles over a) North Bay of Bengal, and b) South Bay of Bengal from 27**
December 2008 to 26 January 2009. Observations are from Bikkina et al. (2020). Aerosol Fe solubility was calculated along the cruise
tracks using the IMPACT model. In Test 0, we run the model without upgrades (Ito et al., 2021) and applying the photoinduced
dissolution scheme for combustion aerosols (Ito, 2015). The proton + oxalate dissolution scheme (Table 1) was applied in Test 1 and
75 **3, while proton-promoted dissolution is used for Test 2. We adopted the mineral-specific inventory for anthropogenic Fe emissions**
(Rathod et al., 2020) in Test 1 and 2. In Test 3, the Fe speciation of Krakow ash was used for all combustion sources. The small white
square within the box shows the mean. The solid line within the box indicates the median. The lower and upper hinges correspond
to the 25th and 75th percentiles. The whiskers above and below the box indicate the 1.5 × interquartile range, and the data outside
this range are plotted individually.

a) Proton-promoted Fe dissolution
pH 2.1 - 0.05 M H₂SO₄, 1 M (NH₄)₂SO₄



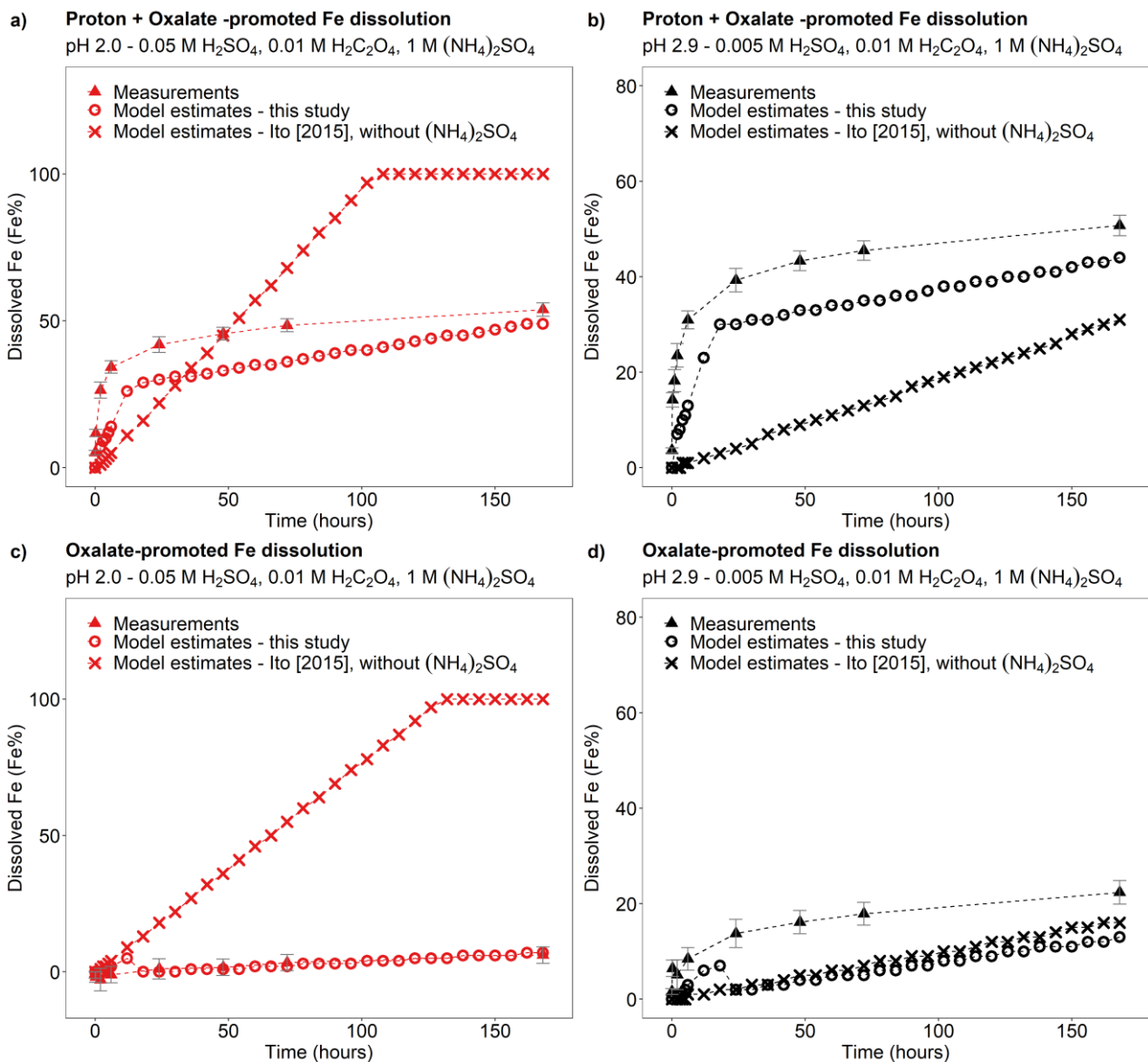
b) Proton-promoted Fe dissolution
pH 3.0 - 0.01 M H₂SO₄, 1 M (NH₄)₂SO₄



80

Figure S8: Comparison between the proton-promoted Fe dissolution of Krakow ash calculated using the original (Ito, 2015) and the new dissolution scheme (Tables 1 and S3). The Fe dissolution kinetics was measured in H₂SO₄ solutions with 1 M (NH₄)₂SO₄ a) at pH 2.1, and b) at pH 3.0 (filled rectangles). The Fe dissolution kinetic was predicted using the rate constants in Table 1 calculated in this study (open circles) and the dissolution scheme for combustion aerosols in Ito (2015) (cross marks). Note that the dissolution scheme in Ito (2015) was calculated based on laboratory measurements conducted at low ionic strength. The molar concentrations of H₂SO₄ and (NH₄)₂SO₄ in the experiment solutions are shown. The final pH of the experiment solutions is also reported, which was calculated using the E-AIM model III for aqueous solution (Wexler and Clegg, 2002) accounting for the buffer capacity of the CFA samples (Experiment 2 at pH 2.1, and Experiment 2 at pH 3.0 in Table S1).

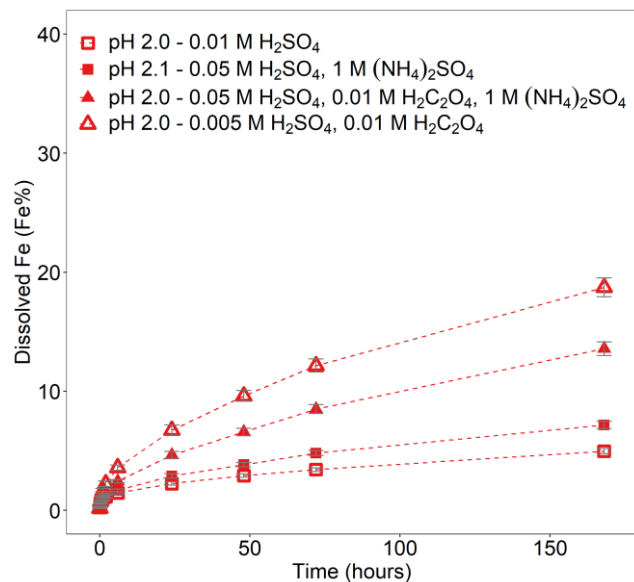
85



90

Figure S9: Comparison between the proton- and oxalate-promoted Fe dissolution of Krakow ash calculated using the original (Ito, 2015) and the new dissolution scheme (Tables 1 and S3). The Fe dissolution kinetics was measured in H₂SO₄ solutions with 0.01 M H₂C₂O₄ and 1 M (NH₄)₂SO₄ a) at pH 2.0, and b) at pH 2.9 (filled triangles). The Fe dissolution kinetic was predicted using the rate constants in Table 1 calculated in this study (open circles) and the dissolution scheme for combustion aerosols in Ito (2015) (cross marks). Note that the dissolution scheme in Ito (2015) was calculated based on laboratory measurements conducted at low ionic strength. c-d) Contribution of the oxalate-promoted dissolution to dissolved Fe estimated using Eq. (3). The molar concentrations of H₂SO₄, H₂C₂O₄ and (NH₄)₂SO₄ in the experiment solutions are shown. The final pH of the experiment solutions is also reported, which was calculated using the E-AIM model III for aqueous solution (Wexler and Clegg, 2002) accounting for the buffer capacity of the CFA samples (Experiment 3 at pH 2.0, and Experiment 3 at pH 2.9 in Table S1).

100



105 **Figure S10:** Fe dissolution kinetics of Libya dust in H₂SO₄ solutions at around pH 2 (open rectangles), with 1 M (NH₄)₂SO₄ (filled rectangles), with 0.01 M H₂C₂O₄ (open triangles), with 0.01 M H₂C₂O₄ and 1 M (NH₄)₂SO₄ (filled triangles). The molar concentrations of H₂SO₄, H₂C₂O₄ and (NH₄)₂SO₄ in the experiment solutions are shown. The final pH of the experiment solutions is also reported, which was calculated using the E-AIM model III for aqueous solution (Wexler and Clegg, 2002) accounting for the buffer capacity of the CFA samples (Experiments 1-4 in Table S1). The data uncertainty was estimated using the error propagation formula.

110 **References**

- Bikkina, S., Kawamura, K., Sarin, M., and Tachibana, E.: ^{13}C Probing of Ambient Photo-Fenton Reactions Involving Iron and Oxalic Acid: Implications for Oceanic Biogeochemistry, *ACS Earth Space Chem.*, 4, 964-976, doi: 10.1021/acsearthspacechem.0c00063, 2020.
- Ito, A.: Atmospheric Processing of Combustion Aerosols as a Source of Bioavailable Iron, *Environ. Sci. Technol. Lett.*, 2, 70-75, doi: 10.1021/acs.estlett.5b00007, 2015.
- Ito, A., Adebiyi, A. A., Huang, Y., and Kok, J. F.: Less atmospheric radiative heating due to aspherical dust with coarser size, *Atmos. Chem. Phys. Discuss.*, 2021, 1-44, doi: 10.5194/acp-2021-134, 2021.
- Rathod, S. D., Hamilton, D. S., Mahowald, N. M., Klimont, Z., Corbett, J. J., and Bond, T. C.: A Mineralogy-Based Anthropogenic Combustion-Iron Emission Inventory, *J. Geophys. Res.-Atmos.*, 125, e2019JD032114, doi: 10.1029/2019jd032114, 2020.
- Wexler, A. S., and Clegg, S. L.: Atmospheric aerosol models for systems including the ions H^+ , NH_4^+ , Na^+ , SO_4^{2-} , NO_3^- , Cl^- , Br^- , and H_2O , *J. Geophys. Res.-Atmos.*, 107, 4207, doi: 10.1029/2001JD000451, 2002.